3D implicit modeling applied to the evaluation of CO_2 geological storage in the shales of the Irati Formation, Paraná Basin, Southeastern Brazil

Saulo B. de Oliveira (sauloboliveira@hotmail.com)
Universidade de São Paulo Instituto de Energia e Meio Ambiente https://orcid.org/0000-0002-2149-1297

Colombo C. G. Tassinari
Universidade de Sao Paulo Instituto de Energia e Ambiente

Richardson M. A-A.
Universidade de Sao Paulo Instituto de Energia e Ambiente

Ignacio Torresi
Seequent Limited

Research Article

Keywords: CO2 geological storage, 3D geological modeling, carbon capture and storage, Irati Formation, Paraná Basin

Posted Date: April 19th, 2021

DOI: https://doi.org/10.21203/rs.3.rs-420789/v1

Version of Record: A version of this preprint was published at Greenhouse Gases: Science and Technology on August 11th, 2021. See the published version at https://doi.org/10.1002/ghg.2111.

Abstract

The Paris Agreement established global ambitious targets for reducing carbon dioxide (CO_2) emissions, requiring the rapid and extensive development of low carbon technologies, and one of the most efficient is CO_2 geological storage. Among the deep geological formations used for CO_2 storage, the shale layers have been a new emerging topic showing to be efficient because they are abundant and have a high content of organic matter, being favorable for CO_2 retention. However, one of the challenges in evaluating a location for possible reservoirs is the adequate geological characterization and storage volume estimates. This research evaluated the Irati Formation of the Paraná Basin, through the information from hydrocarbon exploration wells in Southeastern Brazil, where most stationary sources of carbon emissions are located. Three-dimensional (3D) implicit modeling techniques were applied not only for the volume calculation purpose, but also in the site selection stage, generating thematic 3D models of thickness, depth, structures, and distance to aquifer systems. The limestones, shales, and black shales of the Irati Formation were locally divided into six units according to geological composition and spatial continuity. The E black shale unit was considered for CO_2 geological storage indicating a theoretical capacity of 1.85 Gt of CO_2. The potential of the achieved capacity is promising not only for been greater than the total of CO_2 locally produced but also for supporting the implantation of new projects in this region.

Introduction

In a scenario of growth in the generation and emission of CO_2, the global emissions reached a historical record in the order of 33.1 billion tons (Gt) of CO_2 in 2018 as claimed by the International Energy Agency (IEA 2019). Brazil is among the 20 countries that have emitted the most carbon dioxide in recent years (IEA 2019). Data provided by the *Sistema de Estimativas de Emissões e Remoções de Gases de Efeito Estufa (SEEG)* on CO_2 emissions in the Brazilian energy sector, following the methodology of Azevedo et al. (2018), show an increase from 173 million tons (Mt) of CO_2 in 1990 to 380 Mt of CO_2 in 2018 (SEEG 2020). Brazil has also set goals to contribute to the reduction of GHG emissions, with a reduction of 37% by 2025, and 43% by 2030, based on 2005 emissions, as stated in its Nationally Determined Contribution (NDC) ratification.

This worldwide decision requires the rapid and extensive development of low carbon technologies, and one of the most efficient is Carbon Capture and Storage (CCS). In the Brazilian context, CCS technologies are taking on a relevant space due to the company's performance in the energy sector, mainly due to the development of technologies that respond positively to global trends.

Deep geological formations are an effective alternative for CO_2 storage, but some requirements must be met to allow large amounts of CO_2 to be injected and that the gas remains trapped in the rock for a long

time (Bachu 2000; Miocic et al. 2016). Usually depleted oil and gas fields, saline aquifers, deep salt formations (salt caves and abandoned mines), coal seams, basalt, and black shale layers have been studied as CO_2 reservoirs (IPCC 2005; Orr 2009). Among these, the use of shale layers as a CO_2 reservoir has been a new emerging topic, showing to be efficient because they are abundant and have a high content of organic matter and clay minerals, which are favorable materials for CO_2 retention by adsorption. Besides, the shale layers may contain unconventional gas and oil (shale gas and shale oil) and together with the CO_2 injection, the gas could be produced simultaneously, which allows the process to be more economically viable (Godec et al. 2013b). Shale gas is an energy resource quite extensive globally and their development can consolidate the CO_2 geological storage as a feasible technological alternative to reduce the climate impacts of carbon emissions (Khosrokhavar et al. 2014; Boosari et al. 2015).

This paper aimed to generate a three-dimensional (3D) geological modeling of the Irati Formation, Paraná Basin in a pre-selected area of more than 185,000 km² (Fig. 1) with potential for CO_2 storage in the São Paulo State, southeastern Brazil. The implicit geological modeling in a three-dimensional (3D) virtual environment (Cowan et al. 2002; Cowan et al. 2003; Birch 2014; Jessell et al. 2014) has been widely used in the mineral industry for at least 15 years. However, its use in the other applied areas of geosciences is in growth stages. Few recent examples of 3D implicit geological modeling include iron deposits, as in the Sishen Mine, South Africa (Stoch et al. 2018), base metal deposits, as in Falun, Sweden (Kampmann et al. 2016), Flin Flon, Canada (Schetselaar et al. 2016), Shalipayco, Peru (de Oliveira et al. 2021), gold deposits, as Navachab, Namibia (Vollgger et al. 2015), La Colossa, Colombia (Naranjo et al. 2018), Sigma-Lamaque, Canada (Cowan 2020), and geothermal reservoirs (Alcaraz et al. 2015), amongst others. Its use allows expanding the analysis of conventional geological data by visualizing continuities, groupings, and spatial trends, as well as geometries of geological bodies or units, structural geological framework, and variation of geochemical contents or any other numerical or categorical parameters in geosciences. Recent 3D modeling examples in the oil and gas sector can be seen in Qadri et al. (2019), , Ali et al. (2020), and Islam et al. (2021). Examples of 3D geological modeling focusing on CO_2 storage are scarce, such as Kaufmann and Martin (2008), Douglass and Kelly (2010), Monaghan et al. (2012), Alcalde et al. (2014), Lech et al. (2016), Mediato et al. (2017), Shogenov et al. (2017), Vo Thanh et al. (2019), and Zhong and Carr (2019). Evaluations and studies focusing on CO_2 geological storage in the Paraná Basin include only the study on the Santa Terezinha coal field (Weniger et al. 2010), and the studies considering a saline aquifer (Ketzer et al. 2009; Lima et al. 2011; Rockett et al. 2011; Machado et al. 2013; Dalla Vecchia et al. 2020). The 3D geological model of Paraná Basin can contribute to the assessment of the geological feasibility of implementing CCS technology in Southeastern Brazil, helping to reduce CO_2 in this region where most of the country's carbon emission stationary sources are concentrated (Rockett et al. 2011; Machado et al. 2013; Ketzer et al. 2016). This study considered the hypothesis that the Irati Formation black shales can adsorb significant amounts of CO_2 in compatible capacity with the quantities released in productive activities in the region.

Main Text

GEOLOGICAL SETTING

The Paraná Basin

The Paraná Basin comprises an extensive sedimentation area exceeding 1,000,000 km^2 in southern Brazil holding a stratigraphic record from late Ordovician to Cretaceous and comprising six supersequences (Milani et al. 1998; Milani and Thomaz Filho 2000): Rio Ivaí, Paraná, Gondwana I, Gondwana II, Gondwana III, and Bauru. The Rio Ivaí Supersequence comprises the Alto Garças Formation sandstones, the Iapó Formation diamictites, and the Vila Maria Formation shales and siltstones (Milani et al. 1998). The Paraná Supersequence comprises the continental Furnas Formation sandstones and the marine Ponta Grossa Formation shales (Milani et al. 1998).

The Gondwana I is composed of a basal sequence that includes the glacial sediments of the Itararé Group and the Guatá Group, composed of the Rio Bonito Formation sandstones and coal beds, and the Palermo Formation siltstones and shales. A regressive sequence lies immediately above, consisting of bituminous shale and limestone beds with subordinated evaporite units of the Irati Formation, the Serra Alta Formation shales, the Teresina Formation marine sediments, and the Rio do Rasto Formation red beds, composing the Passa Dois Group (Milani et al. 1998; Milani and Thomaz Filho 2000). The Pirambóia Formation in the northern portion of the Paraná Basin referred to continental sequences up to several hundred meters thick that invaded the Rio do Rasto basin remnants (Milani and Thomaz Filho 2000).

The sediments of the Gondwana II Supersequence are exclusive to the Paraná Basin southernmost portion and are represented by siltstones and sandstones intercalated with red shales of the Santa Maria Formation (Milani et al. 1998). The quartzose sandstones of the Botucatu Formation form the lower portion of the Gondwana III Supersequence, while the upper portion comprises a volcanic sequence up to 2,000 m thick, called Serra Geral Formation that overlies the Paraná Basin rocks and intruded then as sills and dikes (Milani et al. 1998). The Bauru Supersequence is made of deposits with sandy-conglomeratic composition with some silty to shaly deposits that correspond to the Caiuá and Bauru Groups (Milani et al. 1998).

The Parana basin is an intracratonic basin that has a general N-S elongation with a center in the central-west portion, where the fill exceeds 7,000 m in thickness. The most prominent basin structural features are the regional northwest-trending arches of Goiânia, Alto Parnaiba, Ponta Grossa, and Rio Grande, and numerous linear tectonic elements that trend in three major directions: NW-SE mainly, and NE-SW, and E-W subordinately (Zalán et al. 1990). Lineaments in the NW-SE direction are usually wider than the NE-SW structures, and were the preferred ducts for extrusive and intrusive events and are filled by diabase dikes, and also reflects zones of weakness in the basement (Zalán et al. 1990). The NE-trending structures are characterized by faults and fault zones with strike-slip movements, flower structures, and echelon reverse faults and folds. The third group of E-W tectonic lineaments occurs commonly subordinated and secondarily to the first two groups without associated deformation (Zalán et al. 1990).

According to the hydrogeological map of the State of São Paulo (DAEE/IG/IPT/CPRM 2005), in the study region three aquifer systems occur within the Paraná Basin rocks: 1) Bauru Aquifer on the rocks of the Bauru and Caiuá Groups (Silva et al. 2005), 2) Serra Geral Aquifer on the fractured basalts of the Serra Geral Formation (Gastmans et al. 2016), and 3) Guarani Aquifer on the Botucatu and Piramboia Formations (Gilboa et al. 1976; Araújo et al. 1999).

Hydrocarbons in the Paraná Basin

The interest in the Paraná Basin oil potential began in the late 19th century, with the first shallow wells (less than 1,000m) being drilled close to the superficial occurrences of oil in the state of São Paulo. Between 1953 and 1979, Petrobras drilled 60 exploratory wells culminating in the discovery of four sub-commercial accumulations of oil in the Santa Catarina State (Morelatto 2017). In the 1980s, between 1979 and 1983, British Petroleum and Paulipetro companies drilled 30 exploratory wells and discovered the sub-commercial accumulations of natural gas in Cuiabá Paulista, hosted in the Irati Formation, in the far west of São Paulo State (Morelatto 2017). In Fig. 1 and subsequent figures, the Cuiabá Paulista sub-commercial gas accumulation is indicated only by the 3-CB-3-SP well, but in this position, there are also present the 2-CB-1-SP, 2-CB-1DA-SP, 3-CB-2-SP, and 3-CB-4-SP wells, that are distant from each other around 3 km. They were omitted in the figures for a scale issue, avoiding visual pollution with overlapping data.

Between 1986 and 1998 Petrobras retake exploratory activities in the Paraná Basin with the acquisition of new seismic data and with the drilling of seven exploratory wells, which reached the discovery of the Barra Bonita gas field, a structural high trapped at the level of the Itararé Group sandstones (Campos et al. 1998) (Fig. 1). Since 1972 Petrobras operates an oil shale mine in the city of São Mateus do Sul,

Paraná State (Fig. 1). The oil-rich shale of the Irati Formation occurs in two layers in the mine, the lower bituminous has 9.1% oil content and averages about 4.5 m, and the upper has 6.4% and averages about 9 m (Padula 1969; Milani et al. 2007). Currently, with the establishment of the Agência Nacional do Petróleo, Gás Natural e Biocombustíveis (ANP) new surveys and wells have been carried out and areas have been included in bidding rounds in the Paraná Basin (Morelatto 2017).

The Irati Formation

The Irati Formation is the lowermost unit of the Passa Dois Group and occurs in almost every extension of the Paraná Basin, with thickness varying around 40 m with a maximum of 70 m (Holz et al. 2010). Outcrops of the Irati Formation occur mainly along the eastern border (Fig. 2) and at the northern and southern ends of the basin. The lower contact with the sandstones and mudstones of the subjacent Palermo Formation is given by a dark mudstone (Holz et al. 2010). In its top contact, the Irati Formation is superimposed by the Serra Alta Formation shales, and by the Teresina Formation sandstones and siltstones. Abundant sills and dykes generally attributed to the Serra Geral magmatism cut or occur intercalated with Irati Formation rocks.

The composition of the Irati Formation consists of interbedded shales, organic-rich shales, limestones, dolomites, siltstones, and mudstones, with an irregular distribution, distinct lateral continuity, and varying thicknesses along the entire basin (Padula 1968). A subdivision of Irati Formation in two members considers shallow marine siltstones and shales called Taquaral Member in the base, and bituminous black shales intercalated with dolomites, restricted only to the portion northward the Paraná Basin, called Assistência Member in the top (Barbosa and Gomes 1958). Subdivisions of the Irati Formation in seven to eight similar chemostratigraphic units based on geochemical characteristics (identified as A to H units from bottom to top) have been recognized at different locations in the eastern portion of the Paraná Basin (Alferes et al. 2011; Euzébio et al. 2016; Reis et al. 2018; Martins et al. 2020).

DATABASE

The database is composed of hydrocarbon exploration well data provided by ANP in December 2019. The wells were carried out by Petrobras Company during the 1950s until the 2000s. The original individual text file format (.txt) of each well was converted to Excel format (.xlsx) generating a drillhole format database with collar, survey, lithology, stratigraphy, and hydrocarbon spreadsheets. Conventional wireline

logs with gamma-ray, resistivity, density, neutrons, and sonic log of each well were also provided in a reading format file (.pdf). Tables with scanning geochemical data, when available, were provided in a reading format file (.pdf). A filter was applied in a total of 123 wells in the Paraná Basin resulting in 32 wells in the study area (Fig. 1). From these wells, all have stratigraphy data, 29 have some lithology data, and 15 have some hydrocarbon indication data. Almost all filtered wells are vertical with only one having survey data. Then, comma-separated value (.csv) files with the wells data were loaded in the Leapfrog Geothermal® software for performing three-dimensional (3D) geological modeling. The Leapfrog software use radial basis functions (RBFs) to perform surfaces by the implicit modeling method (Cowan et al. 2003). A regional topographic surface was generated from the GTOPO30 data (https://earthexplorer.usgs.gov/). Surface geology data (lithology and structures) were obtained from Companhia de Pesquisa de Recursos Minerais (CPRM) (Lopes et al. 2004) and regional geological structures are from Zalán et al. (1990) and were initially treated in the free software QGIS Desktop before importing into Leapfrog platform.

THE IRATI FORMATION IN THE STUDY AREA

In the study area, outcrops of the Irati Formation are restricted to the southeast portion only (Fig. 2), so the internal unit subdivision came mainly from well data. All wells in the area reached and exceeded the horizon of the Irati Formation, except for the 1-QT-1-PR well, which is very shallow, and the 1-TI-1-SP well, which presents an extensive interval of diabase dike between the Teresina and Palermo Formations (Fig. 3). In the study area, 8 wells (1-J-1-PR, 1-MA-1-SP, 1-PA-1-SP, 1-SA-1-SP, 2-AA-1-SP, 2-AP-1-PR, 2-RI-1-PR, 2-TB-1-SP) present some punctual oil indication, 5 wells present gas indication (2-CB-1-SP, 2-CB-1DA-SP, 3-CB-2-SP, 3-CB-3-SP, 3-CB-4-SP), referring to the Cuiabá Paulista sub-commercial gas accumulations, and 4 wells present bitumen (1-AB-1-SP, 1-GU-4-SP, 2-PN-1-SP, and 2-PP-1-SP), all in Irati Formation intervals (Fig. 2).

A 3D interpretation of the lithology data together with some TOC data enabled a local subdivision of the Irati Formation in units following the subdivision of Euzébio et al. (2016), Reis et al. (2018), and Martins et al. (2020). Due to the erratic availability of samples with TOC analysis, the three A, B, and C base units were undifferentiated and referred to as a single A/B/C shale unit (Fig. 3). So in this work, six units were considered informally named A/B/C shale, D limestone, E black shale, F shale, and H black shale from the bottom to the top (Fig. 3), in order to adapt to the existing division in the literature (Reis et al. 2018). For the interpretation of the units, well intervals less than one meter thick were incorporated (diluted) into the larger adjacent intervals. Thus, shaly units can contain thin and discontinuous levels of limestone, as well as carbonate units, can contain some thin shale levels. The A/B/C unit is a shale layer with local carbonate layers and a high thickness variation from 30 m in the middle of the area to only 3 m in the

eastern portion. The sequence from D to G units is quite continuous laterally and occurs in the entire E-W section (Fig. 3) along the study area for more than 300 km. The D unit consists of limestones, with dolostones locally, which vary from calcilutite to calcarenite with thickness in the wells varying between 1 and 16 m. The thickness from the E black shale unit varies from 2 to 20 m. Both E and F units are interbedded with a diabase sill in the eastern portion. The F unit is composed of shales and has high variable thickness throughout the E-W section (1 to 14 m). The G unit is composed of limestones and dolostones with grain size varying from calcilutite to calcarenite, and with thickness in the wells from 2 to 11 m. The topmost H unit is a black shale layer that occurs only locally in the west of the area. The local Irati Formation subdivision used in this work is similar to the ones seen in outcrops (Fig. 4) and presented in the literature (Reis et al. 2018), although it is not exactly equivalent.

INITIAL CRITERIA FOR SELECTING THE CO_2 STORAGE LOCATION

CO_2 stationary sources and some legal aspects

The macro study area (Fig. 1) already takes into account some criteria for the selection of the CO_2 reservoir location, as the region with the highest occurrence of CO_2 stationary sources and some legal aspects. Excluding the land use, land-use change, and forestry (LULUCF) sector, which is the main net emitter of CO_2 in Brazil, the second sector with the highest emission is energy. The São Paulo State is the state with the highest CO_2 emissions in the energy sector and the highest concentration of thermoelectric power plants in the country (Fig. 1). In 2018 from a total of 380 Mt of CO_2 emitted in the Brazilian energy sector, 80 Mt (21%) refer to the São Paulo State (data from SEEG 2020). The Paraná State also has a high concentration of thermoelectric plants. However, the Paraná State Law 19.878 of 2019 prohibits the production of unconventional natural gas through hydraulic fracking (Ramos et al. 2020), although the state has no oil and gas production activity, not even conventional. The Barra Bonita in the Paraná State is a conventional gas field and is not in production. The legal context of shale gas in the Paraná Basin is better and deeply discussed by Lenhard et al. (2018) and Ramos et al. (2020). The São Paulo State has no legal restrictions or specific legislation for CCS, as well as all over Brazil (Almeida et al. 2017; Costa and Musarra 2020). Therefore, areas inside the São Paulo State were prioritized in this study, mainly because there is also a high concentration of bioenergy industries related to sugar-cane ethanol plants (da Silva et al. 2018).

Regional geological aspects

The Paraná Basin is tectonically related to a more than 10,000km-long divergent margin originated by the Gondwana paleocontinent break-up and the separation of the African and South American plates (Milani and Thomaz Filho 2000), with no relation with fold belts, thus being in a tectonically favorable location for CO_2 reservoir, as recommended by IEA-GHG (2009).

The Paraná Basin in the southeast of Brazil presents a low level of seismic activity, as it is a typically intra-plate region. Only five earthquakes with m_b magnitude above 5.0 (with two being of large-magnitude: 6.3 and 6.8) have occurred in the studied region during the past 220 years according to Berrocal et al. (1996) and the bulletins of Centro de Sismologia da Universidade de São Paulo (USP), Brazil (http://moho.iag.usp.br/eq/bulletin). This scenario characterizes a favorable region for CO_2 reservoir, following IEA-GHG (2009)

Depth, thickness and distance to groundwater aquifers

To evaluate the subsurface depth, thickness, and distance to groundwater aquifers (IEA-GHG 2009), 3D thematic models were built in the Leapfrog platform using lithology data from wells. These models were generated using the *Vein type* software tool. For the depth of the Irati Formation (Fig. 5), all intervals immediately above the formation were selected, and then the model was generated. For the Irati Formation thickness model (Fig. 6) were used the selected wells intervals of the formation itself. For a model of the distance of the CO_2 reservoir until the aquifer systems in the area (Bauru, Serra Geral, and Guarani), it was considered the deepest of them: the Guarani Aquifer, so using the lithology intervals from the top of Irati Formation to the base of the Botucatu and Piramboia Formations (Fig. 7).

The depth of the Irati Formation increases in the western direction towards the depocenters of the basin and can reach more than 2,800 m (Fig. 5). The Irati Formation thickness varies from 22 to 64 m in the wells inside the study area (Fig. 6). In nine wells the Irati Formation thickness has shown outlier values from 94 to 265 m. The respective Irati Formation intervals in the database include some diabase intervals. In the case of these outliers, the data were reclassified considering only the intervals above the diabase. The distance between the top of the Irati Formation and the base of Guarani Aquifer increases in the west direction and can reach more than 1,400 m outside the state of Sao Paulo in the east of the Mato Grosso do Sul state (Fig. 7).

3D IMPLICIT GEOLOGICAL AND STRUCTURAL MODELING

Regional-scale 3D geological and structural model

The 3D geological implicit modeling was built initially on a regional-scale using the previously interpreted stratigraphy data of gamma-ray log, comprising data of geological formations and groups, inside the limits of the study area (Fig. 2). The following 12 geological units were considered in the model, stratigraphically from base to top: Paraná Group, Itararé Group, Rio Bonito Formation, Palermo Formation, Irati Formation, Serra Alta Formation, Teresina Formation, Rio do Rasto Formation, Piramboia Formation, Botucatu Formation, Serra Geral Formation, and Bauru Group. Data from Corumbataí Formation were grouped with Teresina Formation data. The geological contacts from the CPRM geological map were used together with the well data in the East region of the study area, where the geological formations crop out (Lopes et al. 2004). The wells intervals were individually selected and the contact surfaces between each geological formation were generated through the *Deposit type* software tool. Detailed descriptions of the cited software tools are available on the Seequent website (https://help.leapfrog3d.com/Geothermal/). Avoiding any bias or subjective interpretations, the lithological model was exclusively based on well data, with no use of trends or other software artifices. This approach was useful also to identify possible abrupt changes in the stratigraphic sequence that could indicate fault displacements.

The structural model was generated from the surface fault traces (Zalán et al. 1990; Lopes et al. 2004) that have been transformed into fault surfaces assuming a vertical dip for all faults. This assumption is based on a characteristic of extensional regimes, which is the dominance of steeply deep normal faults (Etheridge et al. 1985), following the evolution of the Paraná Basin (Milani and Ramos 1998; Milani and Thomaz Filho 2000). The initial analysis for the site selection looked through regions with less incidence of fractures or faults, avoiding possible CO_2 leaks. The surfaces of the geological contacts were first generated from the contact points of the formations, and then after the fault system was activated in the software generating fault blocks. Due to a large number of faults and lineaments, a process with an empirical approach was applied to activate some faults and analyzing the displacement of blocks case by case. The goal was to locate possible structural traps for CO_2 storage. The final configuration of the structural model generated seven fault blocks (Fig. 8), considering six faults: 1) The Guaxupé Fault with an approximate N60E direction; 2) The Mogi Lineament with an E-W direction; 3) The São Jerônimo Fault with an approximate N40W direction; 4-5) The Santo Anastácio and Guapiara Faults both with a N60W direction, and 6) A local fault with N10E direction limited by the previous two faults.

A structural and stratigraphic trap was identified in Fault Block 4, where there is a structural high with the Irati Formation rocks in contact with the above mudstone-dominated Serra Alta and/or Teresina Formations (Figs. 9 and 10). Inside the domain of Fault Block 4, there is no incidence of any other faults that could allow some possible CO_2 leakage. The Irati Formation in the Fault Block 4 has just over 1,800 km², an average thickness of 38 m, an average depth of 2,640 m, and it is at an average distance of 920 m from the base of the Botucatu Formation (Guarani Aquifer), which is a safe distance because it is greater than the distance of 588 m that was considered by Davies et al. (2012) as the maximum for the propagation of fractures in hydraulic fracking processes, based on thousands of fracture operations performed in the shales of Marcellus, Barnett, Eagle Ford among other fields. The sequence immediately overlying the Irati Formation is the shales and mudstones of the Serra Alta Formation, and then over it, the mudstones interlaminated with fine sandstones of the Teresina Formation (Holz et al. 2010). Considering only the Serra Alta Formation, the caprock thickness is around 65 m, if considered both, Serra Alta and Teresina Formation, the caprock thickness is more than 750 m.

Local 3D geological model

Two wells are located in Fault Block 4: the 1-TI-1-SP and the 2-TB-1-SP. A possible CO_2 reservoir geological model was considered within the Fault Block 4 refining the Irati Formations domain (meshes), considering the previously defined A/B/C to H units (Fig. 12), and a diabase dike that was intercepted by the 1-TI-1-SP well (from 2,854 to 3,140 m). the dike was interpreted as subvertical with the N55W direction, which is the main direction of magnetic lineaments in the area, based on the reduced total field image of magnetic airborne survey (Lopes et al. 2004), and also because it is the preferred direction for intrusions (Zalán et al. 1990). Therefore, the diabase dike divides the Fault Block 4 in two (Fig. 11). The site considered for the possible CO_2 reservoir is on the eastern side of the diabase dike (Fig. 11). Thus, the CO_2 reservoir is bounded by the Mogi Lineament to the north, by the Guapiara Fault to the northeast, by the diabase dike to the southwest, and by a local N10E fault to the southeast, with an area of approximately 1,200 km².

LOCAL ASPECTS OF THE CO_2 RESERVOIR

Porosity and permeability

Table 1 shows the porosity (Φ) and permeability (K) calculated from 2-TB-1-SP well log data for each geological unit of Irati Formation. Porosity derived from the sonic log was based on an equation from Richardson and Tassinari (2019). The values computed for porosity were used to predict the permeability of the layers based on the redefined equations for shale and limestone units (Richardson and Tassinari 2019).

The porosity of the A/B/C and F shale units varies from 8.0 to 16.7%, and the permeability from 0.542 to 75.11 mD, while the porosity of the E and H black shale units have values from 6.1 to 9.2%, and permeability values from 0.088 to 1.383 mD. In the D and G limestone units, the porosity is between 12.6 and 69.0% and the permeability is between 0.567 and 28.41 mD.

Geothermal gradient and temperature

Gomes (2009) presents data of geothermal gradient for Irati Formation calculated through the bottom-hole temperature (BHT) method (Carvalho and Vacquier 1977), for the 2-TB-1-SP well resulting in a gradient of 20.4 ºC/km with a standard deviation of 1.02. The CO_2 reservoir of this study presents a geothermal gradient below 30 ºC/km, as recommended by international literature (IEA-GHG 2009; Miocic et al. 2016). A reservoir in the considered depth of 2,640 m and with this gradient would be at an average temperature of 53.8 ºC, also meeting the recommendation of ≥ 35 ºC (IEA-GHG 2009).

CAPACITY ESTIMATION AND CLASSIFICATION

Among the current CO_2 storage resources, the shale formations have been shown to have the greatest potential, in particular the black shales with TOC content higher than 2% (Levine et al. 2016). The available data of TOC in Irati Formation shale intervals of the 2-TB-1-SP well varies between 0.52 to 9.62% in black shale samples (Table 2). Although the H black shale unit presents higher TOC values (8.45 and 9.62%) than the E unit (0.52 to 7.36%), this last one is considered for capacity calculation due to its greater thickness (20.00 m against 2.00 m) (Table 1 and Fig. 3).

The DOE NETL's equation for shales was utilized for the estimation of the CO_2 mass storage (Levine et al. 2016). Nevertheless, several challenges regarding the storage resource estimation of shale reservoirs are pointed out by Azenkeng et al. (2020). The key factors that control the CO_2 storage in organic-rich shales

are matrix pore spaces, and natural and induced fractures, and it is very difficult to differentiate them (Azenkeng et al. 2020). Table 3 summarizes the variables that were used for calculating the capacity of the E unit shale of Irati Formation inside the Fault Block 4. The calculated porosity of 6.1% from the 2-TB-1-SP well for the E unit (Table 1) refers to natural fractures and pore spaces. The approach assumed for this initial assessment of the Irati Formation shale reservoir was quite conservative, although this study considers hydraulic fracturing to generate fractures and therefore increases porosity, only natural porosity data was used in the calculation. The CO_2 supercritical density of 842.3 kg/m^3 was calculated from the geothermal gradient of 20.4 ºC/km (Gomes 2009) and the average depth of 2.640 m from the 2-TB-1-SP well, and assuming a hydrostatic gradient of 10.7 kPa/m.

Weniger et al. (2010) performed high-pressure experimental sorption isotherms with CO_2 at 45 °C on shale samples from the Irati Formation. The Langmuir sorption model is a limiting model for low pressures, Weniger et al. (2010) applied a modified Langmuir model with an average Langmuir pressure of 15,81 Mpa for the Irati Formation shale samples. Weniger et al. (2010) also recognize a linear correlation between TOC (wt.%) data and the sorption capacities of CO_2, in agreement with results achieved by Nuttal et al. (2005) and Godec et al. (2013a), for the Kentucky shale and the Marcellus Shale, respectively. The CO_2 sorbed mass was calculated using the gradient of 10.7 kPa/m at average depth of 2.640 m, and weighted average TOC of 3.2%, both from 2-TB-1-SP well, using the correlation equations from Weniger et al. (2010).

The volume was directly obtained from the 3D solid of the E black shale unit from the 3D implicit geological model (Table 3). No efficiency factor for the area (E_A) was been applied since some legal surface constraints have been applied previously in the site selection, and by the structural constraints of the limiting faults. The efficiency factor for thickness (E_h) has also not been applied. Although almost all geological parameters such as porosity, temperature, thickness, and TOC come from a single exploration well (2-TB-1-SP), the volume has a considerable level of reliability to be derived from a 3D geological model that was constructed considering also the data of all other 31 wells, geological mapping, topography, and local and regional structures together.

The two efficiency factors from DOE NETL's equation (E_Φ and E_s) were assumed from the simulations of Myshakin et al. (2018), which was based on 60 years of CO_2 injection. The most conservative parameters of P_{10} probability values of 0.15 for E_Φ, and 0.11 for E_s, was considered, reaching 1.85 billion tons of total capacity for the E unit (Table 3). If considered the P_{90} probability values of 0.36 for , and of 0.24 for from Myshakin et al. (2018), the total capacity would be 4.44 billion tons.

For comparison with other organic-rich shale formations, in the Devonian shale in Kentucky, a capacity of 27.7 Gt was estimated at least 304 m deep and 15 m thick (Nuttal et al. 2005), while in the Marcellus Shale a total theoretical capacity of 171.2 Gt was estimated for a depth greater than 915 m (Godec et al. 2013a).

Bachu et al. (2007) proposed a classification considering technical and economic aspects in four categories: theoretical, effective, practical, and matched capacity, according to a gradual level of uncertainty of storage potential. The present study is the initial assessment of the shales of Irati Formation as a CO_2 reservoir, taking into account mainly geological aspects and aiming to provide the basis for a future numerical model study. We assume a Theoretical classification since only a few parameters have already been well defined, such as the seal, depth, geothermal gradient, temperature, and distance to aquifers, which will not vary with the progress of research, all other parameters still need to be refined.

Discussion

Site selection

Table 4 compiles the main parameters used in this study for the determination of the site location of a potential CO_2 reservoir, and evaluation of this reservoir. Concerning seismicity, location in fold belts, complex stratigraphy, and the presence of reservoir-seal pairs for the location of a CO_2 reservoir site (IEA-GHG 2009; Smith et al. 2011; Miocic et al. 2016), the Paraná Basin in Southeastern Brazil presents preferred or favorable results in all aspects. Although in this study, limitations about legal aspects, such as the state legislation of Paraná that prevents hydraulic fracturing had been applied, other topics, like social and environmental issues (Ciotta et al. 2020), still need to be addressed in that region.

The 3D implicit modeling is more robust and has better representativeness of structure and geology than other surface-based methods, improving the modeling accuracy (Cowan et al. 2003; Wellmann and Caumon 2018). The methodology of implicit modeling to build thematic models for depth and thickness of Irati Formation sequence, and for evaluating the distance to protect groundwater, the Guarani Aquifer system, in the study area scale, proved satisfactory and with fast results of easy interpretation (Figs. 5, 6, and 7). The 3D structural model divided the study area into seven fault blocks and defined a structural high (Fault block 4) that conditions a structural and stratigraphic trap (Figs. 8, 9, and 10). These geological aspects of the selected site are favorable for storing carbon because, in addition to having the

sealed siltstones of Serra Alta and Teresina formations above, these siltstones stand side by side with the Irati Formation rocks also acting as lateral barriers for possible gas leaks. The 3D geological models were generated based only on well data and surface or regional geological and structural mapping data, and in that site may exist faults or other structures not visible in the current work scale. Seismic data should be incorporated into that model in future studies to better detail the structural framework.

Reservoir potential

Considering the CO_2 reservoir center of mass of the E black shale unit there are 15 power plants within a radius of 75 km with a total installed capacity of 562 MW. The majority of them, 13 power plants are supplied by biomass, mainly sugarcane bagasse, and the other two power plants by diesel fuel (ANEEL-SIGEL 2020). Increasing the reservoir center radius to 150 km, there are 81 power plants total capacity of 1,625 MW. A biomass power plant with 600 MW capacity emits on average 3.5 million tons of CO_2 per year, according to 2018 base year data from the United States Environmental Protection Agency (EPA 2020). The theoretical capacity of 1.85 Gt of CO_2 reached in the Irati Formation shale would account for the equivalent production of 500 years of only the 75 km radius power plants. Alternatively, applying a simple regression, the CO_2 site location could support up to five times more than the current capacity considering a regional industrial park installation in a long-term horizon of about 68 years, taking into account also the location and the privileged infrastructure of the region. A possible disadvantage concerning the large shale area presented, when projected on the surface, would be the need for extensive terrestrial monitoring, as discussed by Brennan and Burruss (2006) in their comparative study with coal seams versus saline aquifers or depleted reservoirs.

Physical and chemical trapping mechanisms

To maximize storage capacity and the buoyant, the CO_2 is generally injected as a supercritical fluid and is trapped by different physical and chemical trapping mechanisms according to the geological characteristics of each site. In a CO_2 shale reservoir, an adsorption trapping mechanism can permanently store the CO_2 and the shale itself could act as an impermeable barrier and prevent leakage (Kang et al. 2011; Mohagheghian et al. 2019). In addition, to ensure CO_2 retention for a long time, there are immediately above the Irati Formation the shale layers of the Serra Alta Formation, with more than 70 meters thick, which will function as a low permeability sealant layer.

The present study assumes a CO_2 reservoir composed of a unique black shale layer (E unit), however, future studies may consider the entire Irati Formation as a unique hybrid reservoir, contemplating limestones intercalations, with different trapping mechanisms and injectivity conditions. Nevertheless, this evaluation is much broader and requires more extensive detailed characterization studies, which are outside the scope of this research. The focus of this work was to delimit spatially the potential units into the Irati Formation in a 3D environment and provide the basis for subsequent evaluations, what we believe we have achieved. The reached results will be the basis of subsequent studies of mineral characterization of each Irati Formation subdivision defined here and numerical simulations.

Concluding Remarks

1. The Paraná Basin in Southeastern Brazil meets most of the international regional requirements in terms of seismicity, no fold belt, uniform stratigraphy without complex lateral variations, and the presence of reservoir-seal pairs in multi-layered systems.

2. The application of 3D implicit modeling to build thematic models for depth, thickness, structural geology, and distance to protect groundwater, proved satisfactory, and with fast results of easy interpretation. The thematic 3D models were used integrated to define the CO_2 reservoir site.

3. The Irati Formation was locally subdivided into two shale units (A/B/C and F units), two limestone units (D and G units), and two black shale unit (E and H units) in three-dimensional ambient. The E black shale unit was evaluated for CO_2 geological storage.

4. Theoretical capacities calculated for reservoir conditions indicated that an amount of 1.85 Gt of CO_2 could be stored in the organic-rich E shale of the Irati Formation of the Fault Block 4, assuming a CCS project with CO_2 injection as supercritical fluid through hydraulic fracturing.

5. The reached results could be the basis of subsequent studies of mineral characterization of each geological unit of Irati Formation and numerical simulations.

Supplementary Information

Instructions to visualize the 3D model.

To visualize the surfaces in Leapfrog Viewer (as in Fig. 10):

1. Download the free version of the viewer software from https://www.seequent.com/products-solutions/leapfrog-viewer/ and install it.
2. Select “Open Scene”, navigate to the “Irati Formation 3D Geological Model.lfview” file provided and click “Open”.
3. Individual layers can be hidden by clicking on the show/hide “eye” icon on the left hand side and the opacity of objects can be changed using the sliders.

References Cited

Alcalde J, Marzán I, Saura E, Martí D, Ayarza P, Juhlin C, Pérez-Estaún A, Carbonell R (2014) 3D geological characterization of the Hontomín CO2 storage site, Spain: Multidisciplinary approach from seismic, well-log and regional data. Tectonophysics 627:6-25. doi: https://doi.org/10.1016/j.tecto.2014.04.025

Alcaraz S, Chamberfort I, Pearson R, Cantwell A (2015) An integrated approach to 3-D modelling to better understand geothermal reservoirs Proceedings World Geothermal Congress. Melbourne, Australia, pp 19-25

Alferes C, Rodrigues R, Pereira E (2011) Geoquímica orgânica aplicada à Formação Irati, na área de São Mateus do Sul (PR), Brasil. Geochimica Brasiliensis 25:47-54.

Ali M, Abdelmaksoud A, Essa MA, Abdelhady A, Darwish M (2020) 3D Structural, Facies and Petrophysical Modeling of C Member of Six Hills Formation, Komombo Basin, Upper Egypt. Nat Resour Res 29:2575-2597. doi: 10.1007/s11053-019-09583-5

Almeida JRL, Vasconcellos Rocha H, Medeiros Costa H, Santos EM, Rodrigues CF, Sousa MJL (2017) Analysis of civil liability regarding CCS: The Brazilian case. Modern Environmental Science and Engineering 3:382-395. doi: 0.15341/mese(2333-2581)/06.03.2017/003

ANEEL-SIGEL (2020) Data base of the Brazilian Power Sector-SIGEL https://sigel.aneel.gov.br/Down/

Araújo LM, França AB, Potter PE (1999) Hydrogeology of the Mercosul aquifer system in the Paraná and Chaco-Paraná Basins, South America, and comparison with the Navajo-Nugget aquifer system, USA. Hydrogeol J 7:317-336. doi: 10.1007/s100400050205

Azenkeng A, Mibeck BAF, Kurz BA, Gorecki CD, Myshakin EM, Goodman AL, Azzolina NA, Eylands KE, Butler SK, Sanguinito S (2020) An image-based equation for estimating the prospective CO2 storage resource of organic-rich shale formations. International Journal of Greenhouse Gas Control 98:103038. doi: https://doi.org/10.1016/j.ijggc.2020.103038

Azevedo TR, Costa Junior C, Brandão Junior A, Cremer MdS, Piatto M, Tsai DS, Barreto P, Martins H, Sales M, Galuchi T, Rodrigues A, Morgado R, Ferreira AL, Barcellos e Silva F, Viscondi GdF, dos Santos KC, Cunha KBd, Manetti A, Coluna IME, Albuquerque IRd, Junior SW, Leite C, Kishinami R (2018) SEEG

initiative estimates of Brazilian greenhouse gas emissions from 1970 to 2015. Scientific Data 5:180045. doi: 10.1038/sdata.2018.45

Bachu S (2000) Sequestration of CO_2 in geological media: criteria and approach for site selection in response to climate change. Energy Conversion and Management 41:953-970. doi: https://doi.org/10.1016/S0196-8904(99)00149-1

Bachu S, Bonijoly D, Bradshaw J, Burruss R, Holloway S, Christensen NP, Mathiassen OM (2007) CO_2 storage capacity estimation: Methodology and gaps. International Journal of Greenhouse Gas Control 1:430-443. doi: https://doi.org/10.1016/S1750-5836(07)00086-2

Barbosa O, Gomes FdA (1958) Pesquisa de petróleo na bacia do rio Corumbataí, Estado de São Paulo. Ministério da Agricultura, Departamento Nacional da Produção Mineral, Rio de Janeiro.

Berrocal J, Fernandes C, Bassini A, Barbosa JR (1996) Earthquake hazard assessment in southeastern Brazil. Geofísica Internacional 35:257-272.

Birch C (2014) New systems for geological modelling - black box or best practice? Journal of the Southern African Institute of Mining and Metallurgy 114:993-1000.

Boosari SSH, Aybar U, Eshkalak MO (2015) Carbon dioxide storage and sequestration in unconventional shale reservoirs. Journal of Geoscience and Environment Protection 3:7-15.

Brennan ST, Burruss RC (2006) Specific Storage Volumes: A Useful Tool for CO2 Storage Capacity Assessment. Nat Resour Res 15:165-182. doi: 10.1007/s11053-006-9019-0

Campos Ld, Milani E, Toledo M, Queiroz R, Catto A, Selke S (1998) Barra Bonita: a primeira acumulacao comercial de hidrocarboneto da Bacia do Parana, Brasil Rio Oil and Gas Expo and Conference 98. Proceedings of the Rio Oil and Gas Expo and Conference 98, Rio de Janeiro, Brazil, pp 6

Carvalho HDS, Vacquier V (1977) Method for determining terrestrial heat flow in oil fields. Geophysics 42:584-593.

Ciotta M, Peyerl D, Barrozo L, Sant Anna L, Moutinho dos Santos E, Bermann C, Grohmann C, Moretto EM, Tassinari C (2020) An overview of carbon capture and storage atlases around the world. Environ Geosci 27:1-8. doi: https://doi.org/10.1306/eg.10221919015

Costa HKM, Musarra RMLM (2020) Law sources and CCS (carbon capture and storage) regulation in Brazil. International Journal of Advanced Engineering Research and Science 7:196-201. doi: 10.22161/ijaers.72.27

Cowan EJ, Beatson RK, Fright WR, McLennan TJ, Mitchell TJ (2002) Rapid geological modelling Applied Structural Geology for Mineral International Symposium. Kalgoorlie, pp 23-25

Cowan EJ, Beatson RK, Ross HJ, Fright WR, McLennan TJ, Evans TR, Carr JC, Lane RG, Bright DV, Gillman AJ (2003) Practical implicit geological modelling Fifth international mining geology conference. Australian Institute of Mining and Metallurgy Bendigo, Victoria, pp 89-99

Cowan EJ (2020) Deposit-scale structural architecture of the Sigma-Lamaque gold deposit, Canada—insights from a newly proposed 3D method for assessing structural controls from drill hole data. Mineralium Deposita 55:217-240. doi: 10.1007/s00126-019-00949-6

da Silva FTF, Carvalho FM, Corrêa JLG, Merschmann PRdC, Tagomori IS, Szklo A, Schaeffer R (2018) CO_2 capture in ethanol distilleries in Brazil: Designing the optimum carbon transportation network by integrating hubs, pipelines and trucks. International Journal of Greenhouse Gas Control 71:168-183. doi: https://doi.org/10.1016/j.ijggc.2018.02.018

DAEE/IG/IPT/CPRM (2005) Mapa de águas subterrâneas do Estado de São Paulo, escala 1:1.000.000. Nota explicativa. 3 v. edn. Departamento de Águas e Energia Elétrica/ Instituto Geológico/ Instituto de Pesquisas Tecnológicas/ Serviço Geológico do Brasil, São Paulo

Dalla Vecchia F, dos Santos VHJM, Schütz MK, Ponzi GGD, Stepanha ASdGe, Malfatti CdF, Costa EMd (2020) Wellbore integrity in a saline aquifer: Experimental steel-cement interface degradation under supercritical CO2 conditions representative of Brazil's Parana basin. International Journal of Greenhouse Gas Control 98:103077. doi: https://doi.org/10.1016/j.ijggc.2020.103077

Davies RJ, Mathias SA, Moss J, Hustoft S, Newport L (2012) Hydraulic fractures: How far can they go? Marine and Petroleum Geology 37:1-6. doi: https://doi.org/10.1016/j.marpetgeo.2012.04.001

de Oliveira SB, Johnson CA, Juliani C, Monteiro LVS, Leach DL, Caran MGN (2021) Geology and genesis of the Shalipayco evaporite-related Mississippi Valley-type Zn–Pb deposit, Central Peru: 3D geological modeling and C–O–S–Sr isotope constraints. Mineralium Deposita. doi: 10.1007/s00126-020-01029-w

Douglass J, Kelly B (2010) 3D geological modelling and carbon storage potential of the Sydney Basin In: Hutton A, Ward C, Bowman H (eds) Thirty Seventh Symposium on the Geology of the Sydney Basin. Pokolbin, Australia, pp 6-7

EPA (2020) Emissions & generation resource integrated database (eGRID) https://www.epa.gov/energy/egrid,

Etheridge MA, Branson JC, Stuart-Smith PG (1985) Extensional basin-forming structures in Bass Strait and their importance for hydrocarbon exploration. The APPEA Journal 25:344-361.

Euzébio RS, Reis DES, Brito M, Bergamaschi S, Martins MVA, Rodrigues R (2016) Oil generation potential assessment and paleoenvironmental interpretation of Irati Formation (Lower Permian) in northwestern of Paraná Basin (Brazil). Journal of Sedimentary Environments 1:261-274.

Gastmans D, Hutcheon I, Menegário AA, Chang HK (2016) Geochemical evolution of groundwater in a basaltic aquifer based on chemical and stable isotopic data: Case study from the Northeastern portion of Serra Geral Aquifer, São Paulo state (Brazil). J Hydrol 535:598-611. doi: https://doi.org/10.1016/j.jhydrol.2016.02.016

Gilboa Y, Mero F, Mariano IB (1976) The Botucatu aquifer of South America, model of an untapped continental aquifer. J Hydrol 29:165-179. doi: https://doi.org/10.1016/0022-1694(76)90012-3

Godec M, Koperna G, Petrusak R, Oudinot A (2013a) Potential for enhanced gas recovery and CO2 storage in the Marcellus Shale in the Eastern United States. International Journal of Coal Geology 118:95-104. doi: https://doi.org/10.1016/j.coal.2013.05.007

Godec ML, Jonsson H, Basava-Reddi L (2013b) Potential global implications of gas production from shales and coal for geological CO_2 storage. Energy Procedia 37:6656-6666. doi: https://doi.org/10.1016/j.egypro.2013.06.598

Gomes AJL (2009) Avaliação de recursos geotermais da Bacia do Paraná. Observatório Nacional, Rio de Janeiro, pp 170

Holz M, França AB, Souza PA, Iannuzzi R, Rohn R (2010) A stratigraphic chart of the Late Carboniferous/Permian succession of the eastern border of the Paraná Basin, Brazil, South America. Journal of South American Earth Sciences 29:381-399. doi: https://doi.org/10.1016/j.jsames.2009.04.004

IEA-GHG (2009) IEA greenhouse gas R&D programme: CCS Site characterisation criteria In: Bachu S, Hawkes C, Lawton D, Pooladi-Darvish M, Perkins E (eds). Cheltenham, United Kingdom, pp 112

IEA (2019) Global energy & CO_2 status report 2019. Paris

IPCC (2005) Intergovernmental panel on climate change special report on carbon dioxide capture and storage In: Metz B, Davidson O, De Coninck H, Loos M, Meyer L (eds). Intergovernmental Panel on Climate Change, Cambridge, UK and New York, USA, pp 442

Islam MA, Yunsi M, Qadri SMT, Shalaby MR, Haque AKME (2021) Three-Dimensional Structural and Petrophysical Modeling for Reservoir Characterization of the Mangahewa Formation, Pohokura Gas-Condensate Field, Taranaki Basin, New Zealand. Nat Resour Res 30:371-394. doi: 10.1007/s11053-020-09744-x

Jessell M, Aillères L, De Kemp E, Lindsay M, Wellmann JF, Hillier M, Laurent G, Carmichael T, Martin R (2014) Next generation three-dimensional geologic modeling and inversion. Society of Economic Geologists Special Publication 18:261-272.

Kampmann TC, Stephens MB, Weihed P (2016) 3D modelling and sheath folding at the Falun pyritic Zn-Pb-Cu-(Au-Ag) sulphide deposit and implications for exploration in a 1.9 Ga ore district, Fennoscandian Shield, Sweden. Mineralium Deposita 51:665-680. doi: 10.1007/s00126-016-0638-z

Kang SM, Fathi E, Ambrose RJ, Akkutlu IY, Sigal RF (2011) Carbon dioxide storage capacity of organic-rich shales. Spe Journal 16:842-855.

Kaufmann O, Martin T (2008) 3D geological modelling from boreholes, cross-sections and geological maps, application over former natural gas storages in coal mines. Computers & Geosciences 34:278-290. doi: https://doi.org/10.1016/j.cageo.2007.09.005

Ketzer JM, Iglesias R, Einloft S, Dullius J, Ligabue R, de Lima V (2009) Water–rock–CO2 interactions in saline aquifers aimed for carbon dioxide storage: Experimental and numerical modeling studies of the Rio Bonito Formation (Permian), southern Brazil. Applied Geochemistry 24:760-767. doi: https://doi.org/10.1016/j.apgeochem.2009.01.001

Ketzer JMM, Machado CX, Rockett GC, Iglesias RS (2016) Atlas brasileiro de captura e armazenamento geológico de CO_2. EDIPUCRS, Porto Alegre, pp 95.

Khosrokhavar R, Griffiths S, Wolf K-H (2014) Shale gas formations and their potential for carbon storage: opportunities and outlook. Environmental Processes 1:595-611. doi: 10.1007/s40710-014-0036-4

Lech ME, Jorgensen DC, Southby C, Wang L, Nguyen V, Borissova I, Lescinsky D (2016) Palaeogeographic mapping to understand the hydrocarbon and CO2 storage potential of the post-rift Warnbro Group, offshore Vlaming Sub-basin, southern Perth Basin, Australia. Marine and Petroleum Geology 77:1206-1226. doi: https://doi.org/10.1016/j.marpetgeo.2016.03.014

Lenhard LG, Andersen SM, Coimbra-Araújo CH (2018) Energy-Environmental Implications Of Shale Gas Exploration In Paraná Hydrological Basin, Brazil. Renewable and Sustainable Energy Reviews 90:56-69. doi: https://doi.org/10.1016/j.rser.2018.03.042

Levine JS, Fukai I, Soeder DJ, Bromhal G, Dilmore RM, Guthrie GD, Rodosta T, Sanguinito S, Frailey S, Gorecki C, Peck W, Goodman AL (2016) U.S. DOE NETL methodology for estimating the prospective CO2 storage resource of shales at the national and regional scale. International Journal of Greenhouse Gas Control 51:81-94. doi: https://doi.org/10.1016/j.ijggc.2016.04.028

Lima Vd, Einloft S, Ketzer JM, Jullien M, Bildstein O, Petronin J-C (2011) CO_2 Geological storage in saline aquifers: Paraná Basin caprock and reservoir chemical reactivity. Energy Procedia 4:5377-5384. doi: https://doi.org/10.1016/j.egypro.2011.02.521

Lopes RC, Peruffo N, Sachs LLB, Silva VA, I.H. B (2004) Folha SF 22 Paranapanema In: Schobbenhaus C, Gonçalves JH, Santos JOS, Abram MB, Leão Neto R, Matos GMM, Vidotti RM, Ramos MAB, Jesus JDAd

(eds) Carta Geológica do Brasil ao Milionémo, Sistema de Informações Geográficas Programa Geologia do Brasil. CPRM, Brasilia.

Machado CX, Rockett GC, Ketzer JMM (2013) Brazilian renewable carbon capture and geological storage map: Possibilities for the Paraná Basin. Energy Procedia 37:6105-6111. doi: https://doi.org/10.1016/j.egypro.2013.06.539

Martins LL, Schulz H-M, Severiano Ribeiro HJP, Nascimento CAd, Souza ESd, da Cruz GF (2020) Organic geochemical signals of freshwater dynamics controlling salinity stratification in organic-rich shales in the Lower Permian Irati Formation (Paraná Basin, Brazil). Org Geochem 140:103958. doi: https://doi.org/10.1016/j.orggeochem.2019.103958

Mediato JF, García-Crespo J, Izquierdo E, García-Lobón JL, Ayala C, Pueyo EL, Molinero R (2017) Three-dimensional Reconstruction of the Caspe Geological Structure (Spain) for Evaluation as a Potential CO2 Storage Site. Energy Procedia 114:4486-4493. doi: https://doi.org/10.1016/j.egypro.2017.03.1608

Milani EJ, Faccini UF, Scherer CM, Araújo LMd, Cupertino JA (1998) Sequences and stratigraphic hierarchy of the Paraná Basin (Ordovician to Cretaceous), southern Brazil. Boletim IG-USP 29:125-173.

Milani EJ, Ramos VA (1998) Orogenias paleozóicas no domínio sul-ocidental do Gondwana e os ciclos de subsidência da Bacia do Paraná. Revista Brasileira de Geociências 28:473-484.

Milani EJ, Thomaz Filho A (2000) Sedimentary basins of South America In: Cordani UG, Milani EJ, Thomaz Filho A, Campos DA (eds) Tectonic Evolution of South America. In-Fólio Produção Editorial, , Rio de Janeiro, Brazil, pp 389-449.

Milani EJ, França AB, Medeiros RA (2007) Rochas geradoras e rochas-reservatório da Bacia do Paraná, faixa oriental de afloramentos, Estado do Paraná. Roteiros Geológicos. Boletim de Geociências da Petrobras 15:135-162.

Miocic JM, Gilfillan SMV, Roberts JJ, Edlmann K, McDermott CI, Haszeldine RS (2016) Controls on CO2 storage security in natural reservoirs and implications for CO2 storage site selection. International Journal of Greenhouse Gas Control 51:118-125. doi: https://doi.org/10.1016/j.ijggc.2016.05.019

Mohagheghian E, Hassanzadeh H, Chen Z (2019) CO_2 sequestration coupled with enhanced gas recovery in shale gas reservoirs. Journal of CO_2 Utilization 34:646-655. doi: https://doi.org/10.1016/j.jcou.2019.08.016

Monaghan A, Ford J, Milodowski A, McInroy D, Pharaoh T, Rushton J, Browne M, Cooper A, Hulbert A, Napier B (2012) New insights from 3D geological models at analogue CO_2 storage sites in Lincolnshire and eastern Scotland, UK. Proc Yorkshire Geol Soc 59:53. doi: https://doi.org/10.1144/pygs.59.1.289

Morelatto R (2017) Bacia do Paraná - Sumário Geológico e Setores em Oferta Rodada Brasil 15, Concessões de Petróleo e Gás. Agência Nacional do Petróleo, Gás Natural e Biocombustíveis (ANP), Rio de Janeiro, pp 18

Myshakin EM, Singh H, Sanguinito S, Bromhal G, Goodman AL (2018) Numerical estimations of storage efficiency for the prospective CO2 storage resource of shales. International Journal of Greenhouse Gas Control 76:24-31. doi: https://doi.org/10.1016/j.ijggc.2018.06.010

Naranjo A, Horner J, Jahoda R, Diamond LW, Castro A, Uribe A, Perez C, Paz H, Mejia C, Weil J (2018) La Colosa Au Porphyry Deposit, Colombia: Mineralization Styles, Structural Controls, and Age Constraints. Econ Geol 113:553-578.

Nuttal BC, Eble C, Bustin RM, Drahovzal JA (2005) - Analysis of Devonian black shales in kentucky for potential carbon dioxide sequestration and enhanced natural gas production In: Rubin ES, Keith DW, Gilboy CF, Wilson M, Morris T, Gale J, Thambimuthu K (eds) Greenhouse Gas Control Technologies 7. Elsevier Science Ltd, Oxford, pp 2225-2228.

Orr FM (2009) Onshore Geologic Storage of CO_2. Science 325:1656. doi: 10.1126/science.1175677

Padula VT (1968) Estudos geológicos da Formação Irati, sul do Brasil. Boletim Técnico da Petrobrás 11:407-430.

Padula VT (1969) Oil Shale of Permian Iratí Formation, Brazil1. AAPG Bull 53:591-602. doi: 10.1306/5D25C69F-16C1-11D7-8645000102C1865D

Qadri SMT, Islam MA, Shalaby MR (2019) Three-Dimensional Petrophysical Modelling and Volumetric Analysis to Model the Reservoir Potential of the Kupe Field, Taranaki Basin, New Zealand. Nat Resour Res 28:369-392. doi: 10.1007/s11053-018-9394-3

Ramos KN, Petry PM, de Medeiros Costa HK (2020) ATUALIZAÇÕES DA EXPLORAÇÃO DE GÁS NÃO CONVENCIONAL NO BRASIL. Revista Gestão & Sustentabilidade Ambiental 9:237-258.

Reis DES, Rodrigues R, Moldowan JM, Jones CM, Brito M, Costa Cavalcante D, Portela HA (2018) Biomarkers stratigraphy of Irati Formation (Lower Permian) in the southern portion of Paraná Basin (Brazil). Marine and Petroleum Geology 95:110-138. doi: https://doi.org/10.1016/j.marpetgeo.2018.04.007

Richardson MA-A, Tassinari CCG (2019) Total organic carbon, porosity and permeability correlation: A tool for carbon dioxide storage potential evaluation in Irati Formation of the Parana Basin, Brazil. Energy and Environmental Engineering 13:602-606.

Rockett GC, Machado CX, Ketzer JMM, Centeno CI (2011) The CARBMAP project: Matching CO2 sources and geological sinks in Brazil using geographic information system. Energy Procedia 4:2764-2771. doi:

https://doi.org/10.1016/j.egypro.2011.02.179

Schetselaar E, Pehrsson S, Devine C, Lafrance B, White D, Malinowski M (2016) 3-D geologic modeling in the Flin Flon mining district, Trans-Hudson orogen, Canada: Evidence for polyphase imbrication of the Flin Flon-777-Callinan volcanogenic massive sulfide ore system. Econ Geol 111:877-901.

SEEG (2020) Sistema de Estimativas de Emissões e Remoções de Gases de Efeito Estufa http://seeg.eco.br/

Shogenov K, Forlin E, Shogenova A (2017) 3D Geological and Petrophysical Numerical Models of E6 Structure for CO2 Storage in the Baltic Sea. Energy Procedia 114:3564-3571. doi: https://doi.org/10.1016/j.egypro.2017.03.1486

Silva FdP, Kiang CH, Caetano-Chang MR (2005) Hidroestratigrafia do Grupo Bauru (K) no Estado de São Paulo. Águas Subterrâneas 19:18. doi: https://doi.org/10.14295/ras.v19i2.8225

Smith M, Campbell D, Mackay E, Polson D (2011) CO_2 aquifer storage site evaluation and monitoring: Understanding the challenges of CO_2 storage: results of the CASSEM project. Scottish Carbon Capture and Storage (SCCS), Heriot-Watt University, Edimburgh.

Stoch B, Anthonissen CJ, McCall MJ, Basson IJ, Deacon J, Cloete E, Botha J, Britz J, Strydom M, Nel D, Bester M (2018) 3D implicit modeling of the Sishen Mine: new resolution of the geometry and origin of Fe mineralization. Mineralium Deposita 53:835-853. doi: 10.1007/s00126-017-0784-y

Vo Thanh H, Sugai Y, Nguele R, Sasaki K (2019) Integrated workflow in 3D geological model construction for evaluation of CO2 storage capacity of a fractured basement reservoir in Cuu Long Basin, Vietnam. International Journal of Greenhouse Gas Control 90:102826. doi: https://doi.org/10.1016/j.ijggc.2019.102826

Vollgger SA, Cruden AR, Ailleres L, Cowan EJ (2015) Regional dome evolution and its control on ore-grade distribution: Insights from 3D implicit modelling of the Navachab gold deposit, Namibia. Ore Geology Reviews 69:268-284. doi: https://doi.org/10.1016/j.oregeorev.2015.02.020

Wellmann F, Caumon G (2018) Chapter One - 3-D Structural geological models: Concepts, methods, and uncertainties In: Schmelzbach C (ed) Adv Geophys. Elsevier, pp 1-121.

Weniger P, Kalkreuth W, Busch A, Krooss BM (2010) High-pressure methane and carbon dioxide sorption on coal and shale samples from the Paraná Basin, Brazil. International Journal of Coal Geology 84:190-205. doi: https://doi.org/10.1016/j.coal.2010.08.003

Zalán PV, Wolff S, Astolfi MAM, Vieira IS, Concelcao JCJ, Appi VT, Neto EVS, Cerqueira JR, Marques A (1990) The Parana Basin, Brazil: Chapter 33: Part II. Selected Analog Interior Cratonic Basins: Analog

Basins In: Leighton MW, Kolata DR, Oltz DF, Eidel JJ (eds) Interior Cratonic Basins. AAPG, Tulsa, USA, pp 681-708.

Zhong Z, Carr TR (2019) Geostatistical 3D geological model construction to estimate the capacity of commercial scale injection and storage of CO2 in Jacksonburg-Stringtown oil field, West Virginia, USA. International Journal of Greenhouse Gas Control 80:61-75. doi: https://doi.org/10.1016/j.ijggc.2018.10.011

Tables

Table 1. Rock type, thickness, porosity (), and permeability (K) data for each unit of Irati Formation in the 2-TB-1-SP well.

Unit	Rock type	Thickness (m)		K (mD)
H	Black shale	2.00	0.092	1.383
G	Limestone	4.00	0.690	0.567
F	Shale	1.00	0.080	0.542
E	Black shale	20.0	0.061	0.088
D	Limestone	5.00	0.126	28.41
A/B/C	Shale	7.00	0.167	75.11

Table 2. Total organic carbon (TOC wt.%) data on the Irati Formation intervals in the 2-TB-1-SP well, with the geological unit subdivision of this study.

Top	Bottom	Rock type	Unit	TOC wt.%
2,618.94	2,619.94	Black shale	H	8.45
2,620.00	2,621.00	Black shale	H	9.62
2,622.94	2,623.94	Limestone	G	2.02
2,623.94	2,624.94	Shale	F	1.44
2,624.94	2,625.95	Black shale	E	7.36
2,628.32	2,629.32	Black shale	E	7.26
2,631.32	2,632.32	Black shale	E	4.53
2,632.32	2,633.42	Black shale	E	2.88
2,633.42	2,633.82	Black shale	E	5.03
2,633.82	2,635.32	Black shale	E	2.45
2,635.32	2,636.32	Black shale	E	0.52
2,637.32	2,637.90	Black shale	E	1.15
2,640.00	2,646.00	Black shale	E	2.25
2,649.00	2,652.00	Limestone	D	1.51
2,653.40	2,654.40	Shale	A/B/C	0.19
2,656.28	2,657.28	Shale	A/B/C	0.28

Table 3. Theoretical CO_2 storage for the E black shale unit of the Irati Formation.

Symbol	Unit	Parameters	Value
v	m^3	volume	23,914,000,000
Φ	%	porosity	6.1%
$\rho CO2$	kg/m^3	CO_2 density at reservoir conditions	842.3
ρs_{CO2}	kg/m^3	mass of CO_2 sorbed per unit volume of solid rock	0.31
E_Φ	%	free phase storage efficiency factor	0.15%
E_s	%	sorption efficiency factor	0.11%
M_{CO2}	Gt	mass of CO_2	1.85

Table 4. Site selection criteria for geological CO_2 storage and our study results.

Criterion	Eliminatory or unfavourable	Preferred or Favourable	Reference	This study
Reservoir-seal pairs; extensive and competent barrier to vertical flow	Poor, discontinuous, faulted and/or breached	Intermediate and excellent; many pairs (multi-layered system)	IEA-GHG, 2009	Vertically sealing faults, multi-layered systems
	-	Vertically sealing faults, multi-layered systems	Miocic et al., 2016	
Stratigraphy	Complex lateral variation and complex connectivity	Uniform	Smith et al., 2011	Uniform
Located within fold belts	Yes	No	IEA-GHG, 2009	No
Seismicity	High	Moderate and less	IEA-GHG, 2009	Low
Depth	< 800 m or > 2,500 m	Between 1,000 and 2,500 m	Chadwick et al. 2008	Average depth 2,640 m
	< 750-800 m	> 800 m	IEA-GHG, 2009	
	< 800 m > 2,500m	> 800 m < 2,500 m	Smith et al., 2011	
	-	> 1,200 m	Miocic et al., 2016	
Thickness	< 20 m	> 50 m	Chadwick et al. 2008	Average thickness 20 m
	< 20 m	≥ 20 m	IEA-GHG, 2009	
Affecting protected groundwater quality	Yes	No	IEA-GHG, 2009	Distance of 920m to aquifer system
Faulting and fracturing intensity		Small or no faults	Chadwick et al. 2008	Minimal faulting, with trapping structure
	Extensive	Limited to moderate	IEA-GHG, 2009	
		Minimal faulting, with trapping structure	Smith et al., 2011	
Caprock thickness	< 20 m	> 100 m	Chadwick et al. 2008	> 750 m (Serra Alta 64 m thick + Teresina Formations 690 m thick)
	< 10 m	≥ 10 m	IEA-GHG, 2009	
	< 20 m thick	> 100 m thick	Smith et al., 2011	
	-	> 150m	Miocic et al., 2016	
Lateral continuity of caprock	Lateral variations, faulted	Unfaulted (Uniform)	Chadwick et al. 2008	Unfaulted
Porosity	< 10%	> 20%	Chadwick et al. 2008	6.1%
	< 10%	≥ 10%	IEA-GHG, 2009	
	< 10%	> 20%	Smith et al., 2011	
Geothermal regime	Gradients ≥ 35 ºC/km and/or high surface	Gradients < 35 ºC/km and low	IEA-GHG, 2009	20.4 ºC/km

	temperature -	surface temperature Geo-thermal gradient of max. 30 ºC/km	Miocic et al., 2016	
Temperature	< 35 ºC	≥ 35 ºC	IEA-GHG, 2009	54 ºC
Total organic organic carbon	< 2.0%	≥ 2.0%	Goodman et al., 2014	3.15%
Well density	High	Low to moderate	IEA-GHG, 2009	Low
Proximity to powerplant	> 100 km	< 75 km	Smith et al., 2011	15 powerplants (562 MW) within a radius of 75 km
Total storage capacity	Total capacity estimated to be similar to or less than the total amount produced from the CO source	Total capacity estimated to be much larger than the total amount produced from the CO_2	Chadwick et al. 2008	Total capacity estimated to be much larger than the total amount produced from the CO_2

Figures

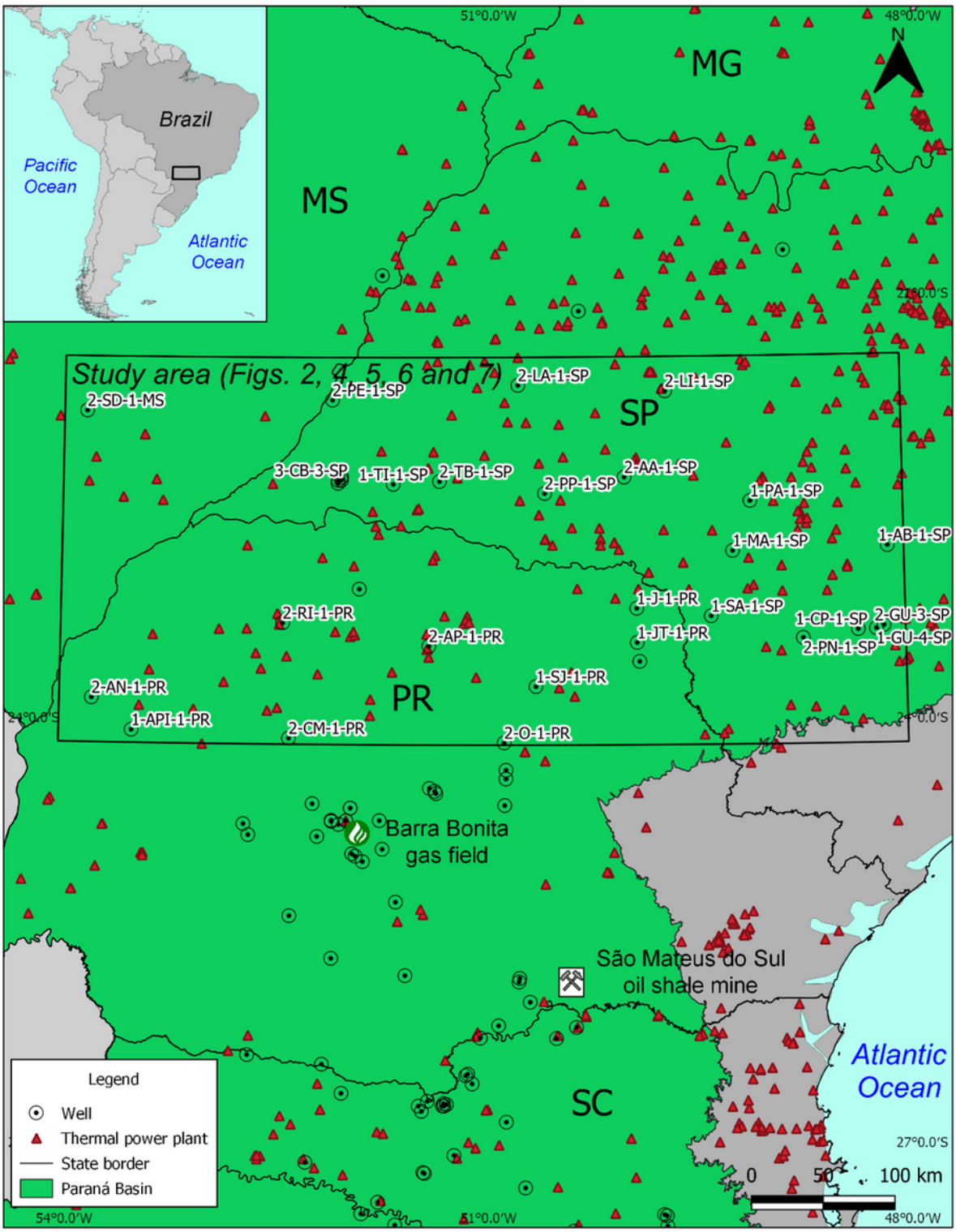

Figure 1

Location of wells, thermoelectric power plants, and the study area in the central Paraná Basin. Power plants' locations are from ANEEL-SIGEL (2020). MG = Minas Gerais State, MS = Mato Grosso do Sul State, PR = Paraná State, SC = Santa Catarina State, SP = São Paulo State.

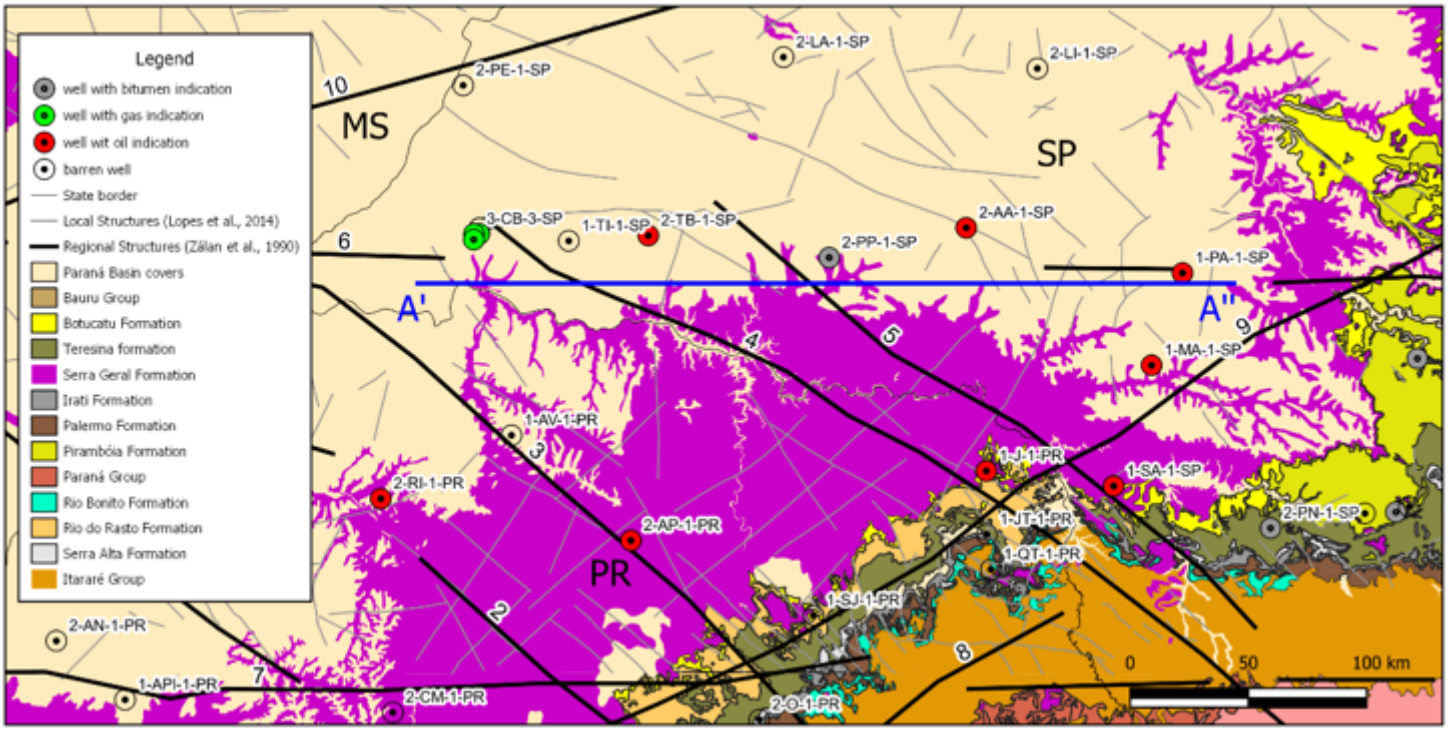

Figure 2

Geological map of the study area with local structures (Lopes et al. 2004), and main regional structures (Zalán et al. 1990). Location of the schematic geological section (A'-A") of Fig. 3. 1 - Cândido Fault, 2 - Curitiba Fault Zone, 3 - São Jerônimo Fault, 4 - Santo Anastácio Fault, 5 – Guapiara Fault Zone, 6 - Mogi Lineament, 7 - São Sebastião Lineament, 8 - Jacutinga Fault, 9 - Guaxupé Fault, 10 - Araçatuba Lineament.

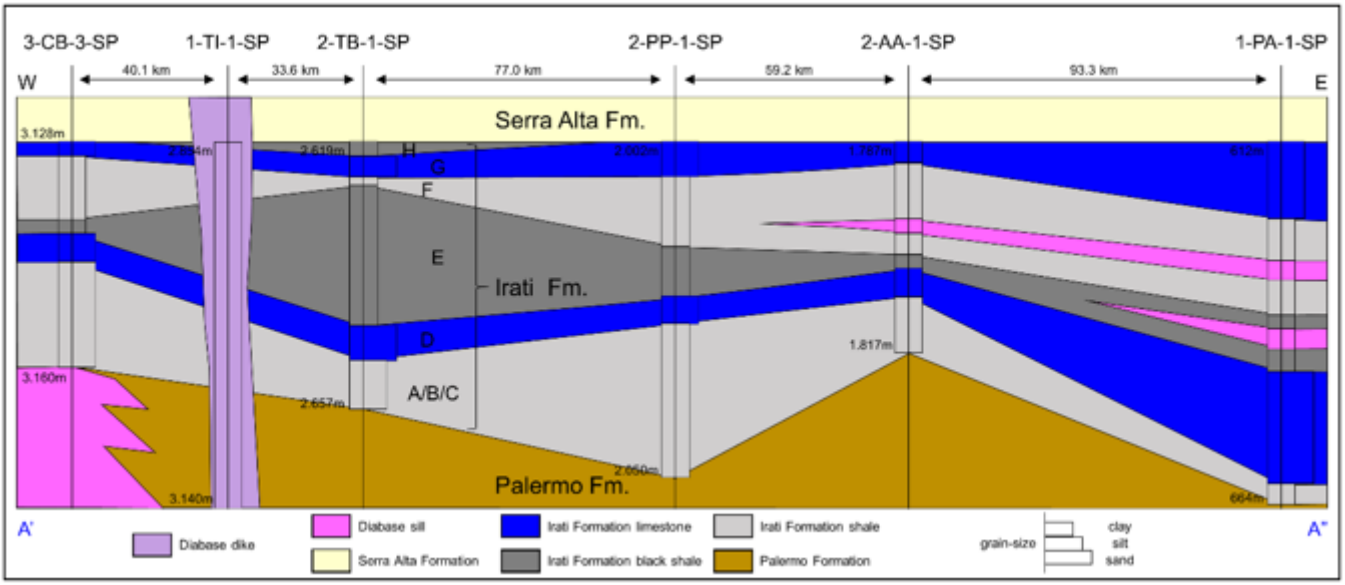

Figure 3

Schematic geological section of the Irati Formation with a local subdivision in six geological units: A/B/C shale, D limestone, E black shale, F shale, G limestone, and H black shale.

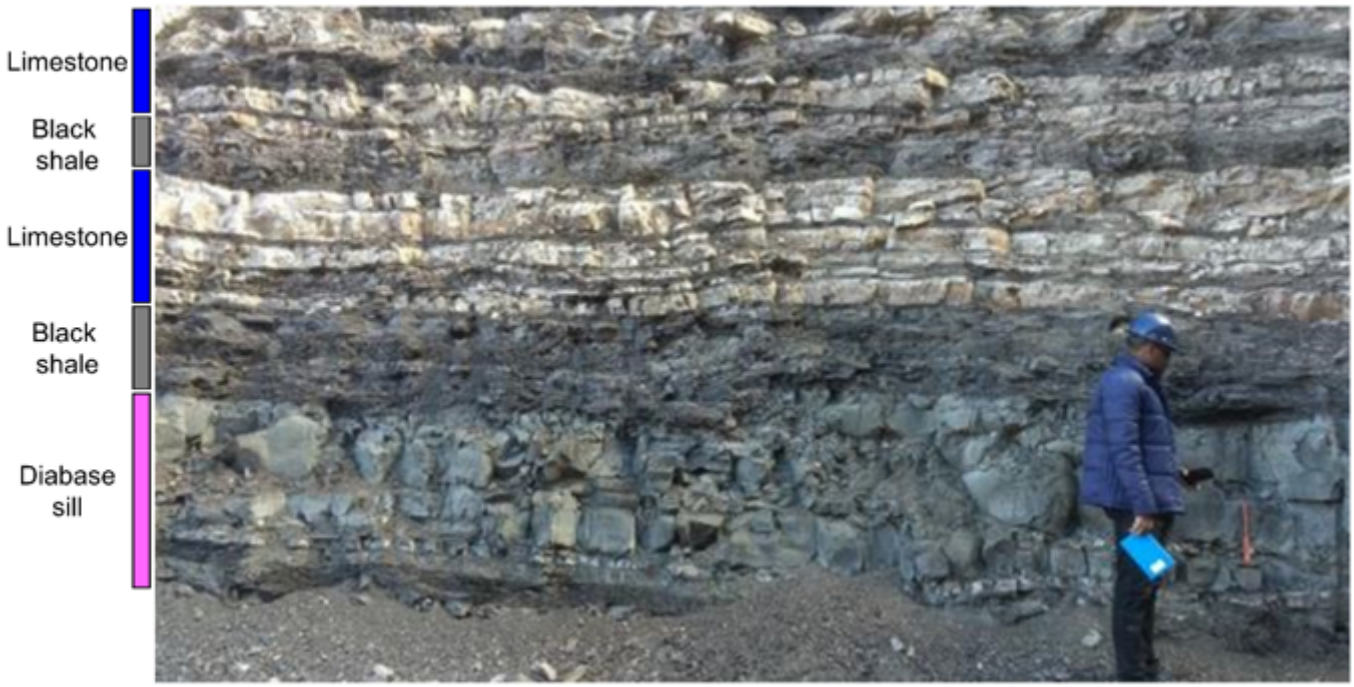

Figure 4

Intercalations of shale and limestone layers of Irati Formation in the Elba Quarry, Northwest of Paraná Basin.

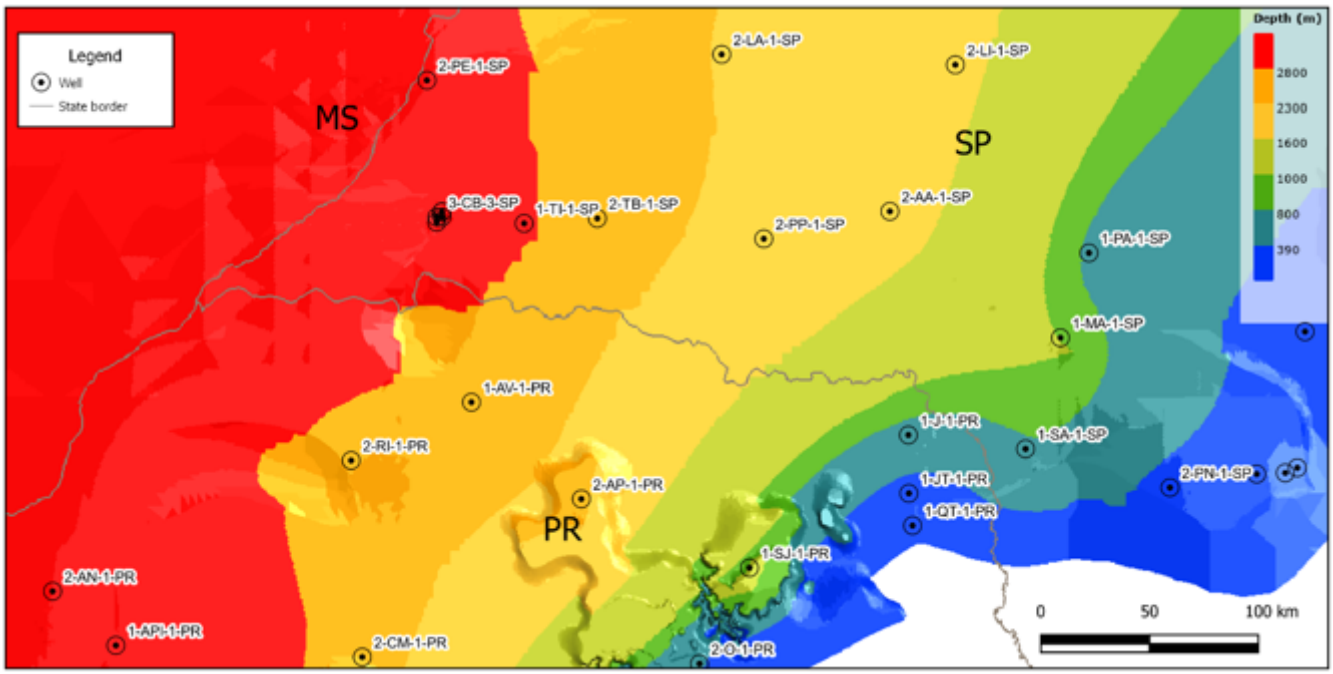

Figure 5

Plan view of the Irati Formation depth model in the study area.

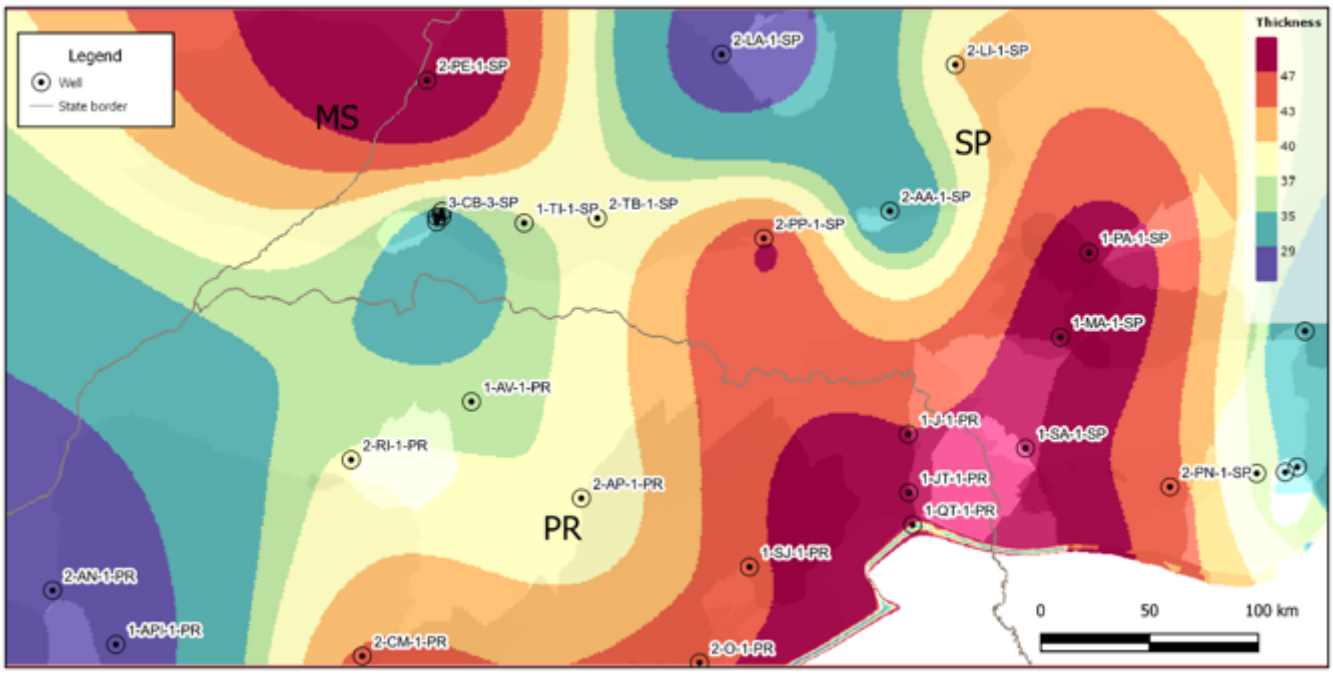

Figure 6

Plan view of the Irati Formation thickness model in the study area.

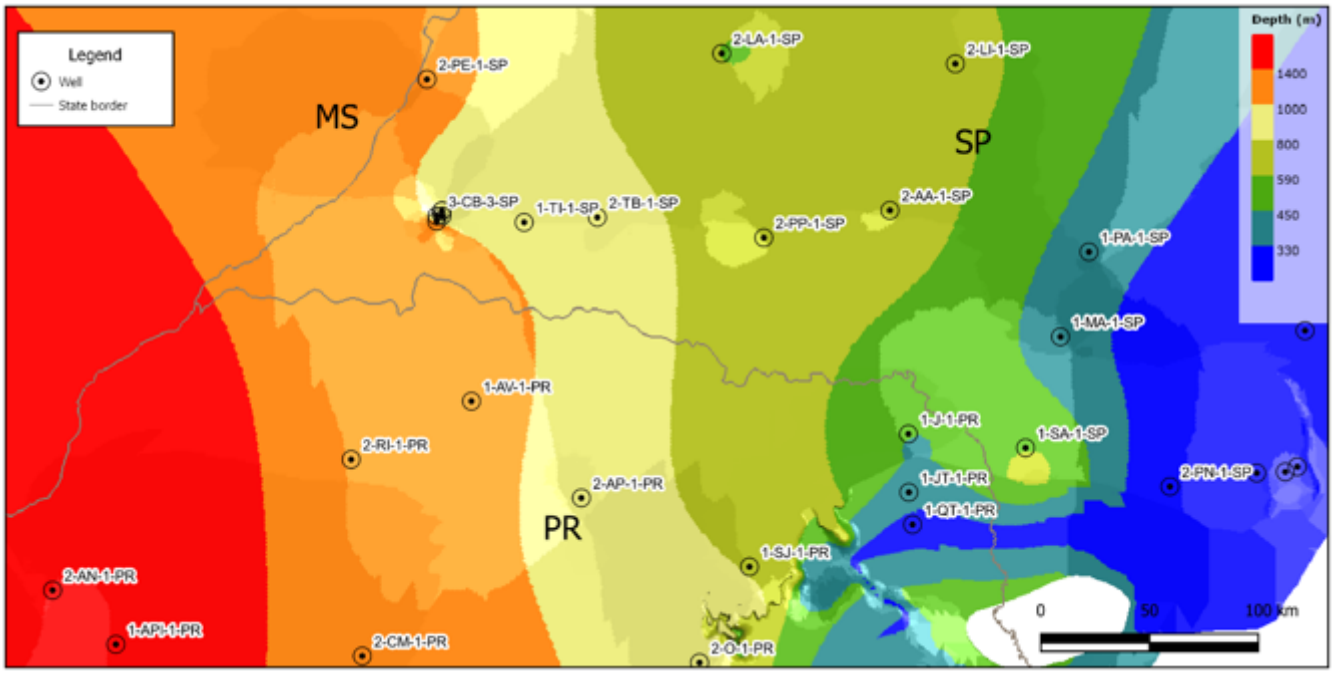

Figure 7

Plan view of the model of the distance from the top of the Irati Formation to the base of the Guarani Aquifer in the study area.

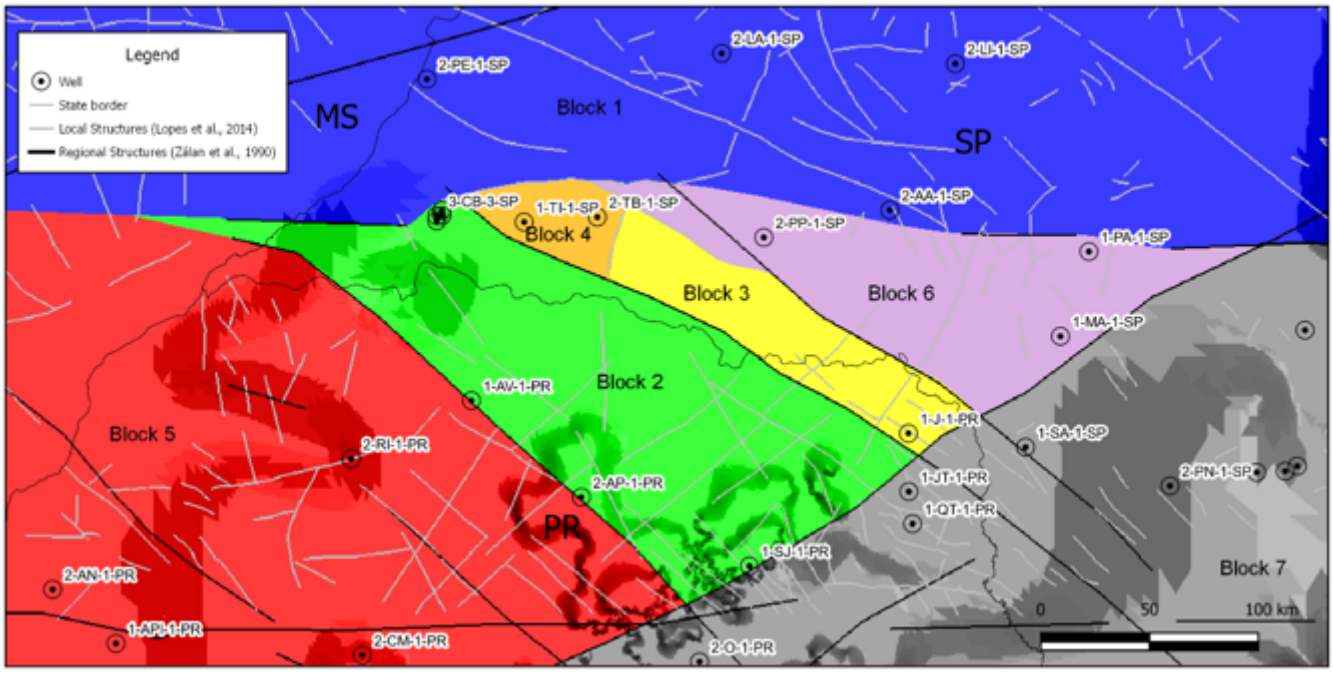

Figure 8

Plan view of the structural model showing the seven fault blocks defined by the main regional structures in the study area.

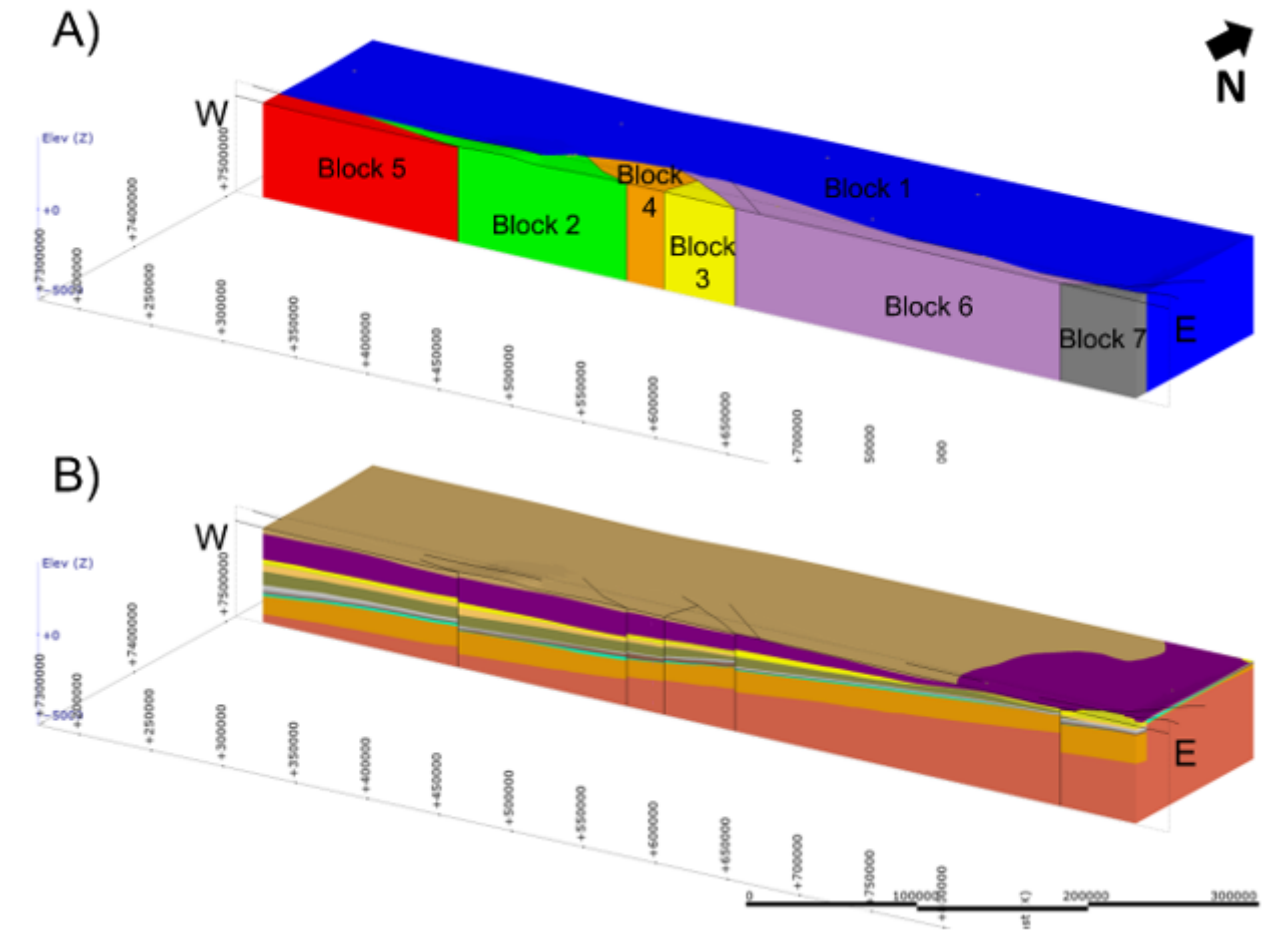

Figure 9

3D view with an E-W slice. A) Structural fault blocks. B) Structural geological model. The legend color is the same as in Fig. 2. Vertical scale = 10x.

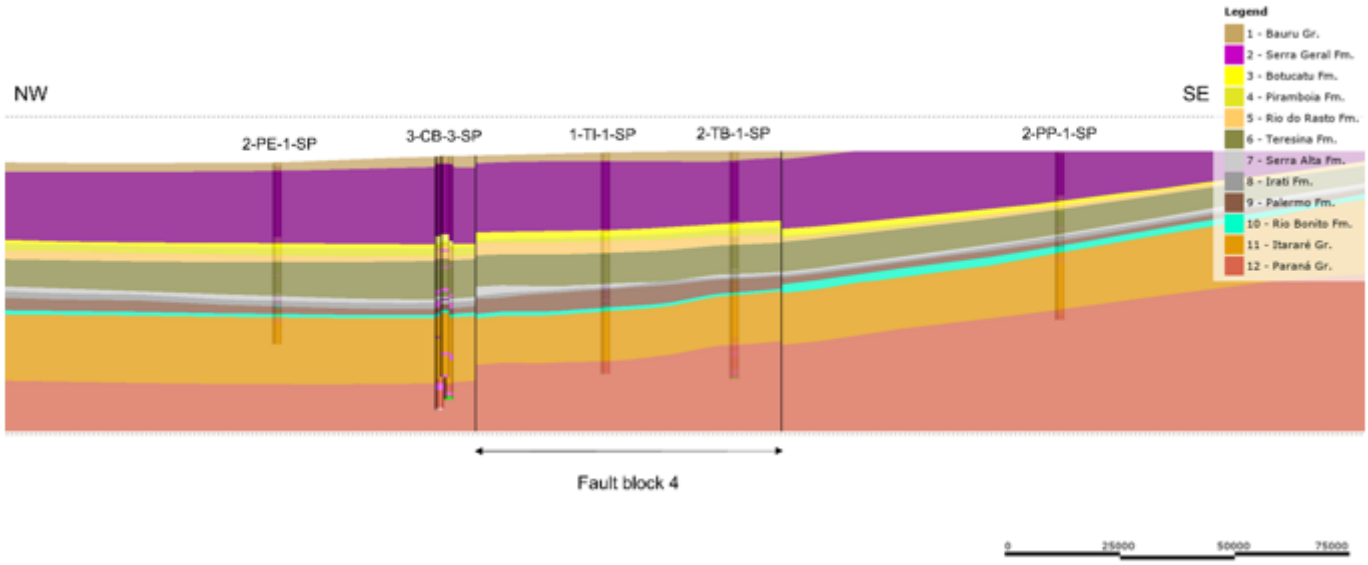

Figure 10

NW-SE section view of the 3D structural and geological modeling highlighting the Fault Block 4 as a structural high. Vertical scale = 10x.

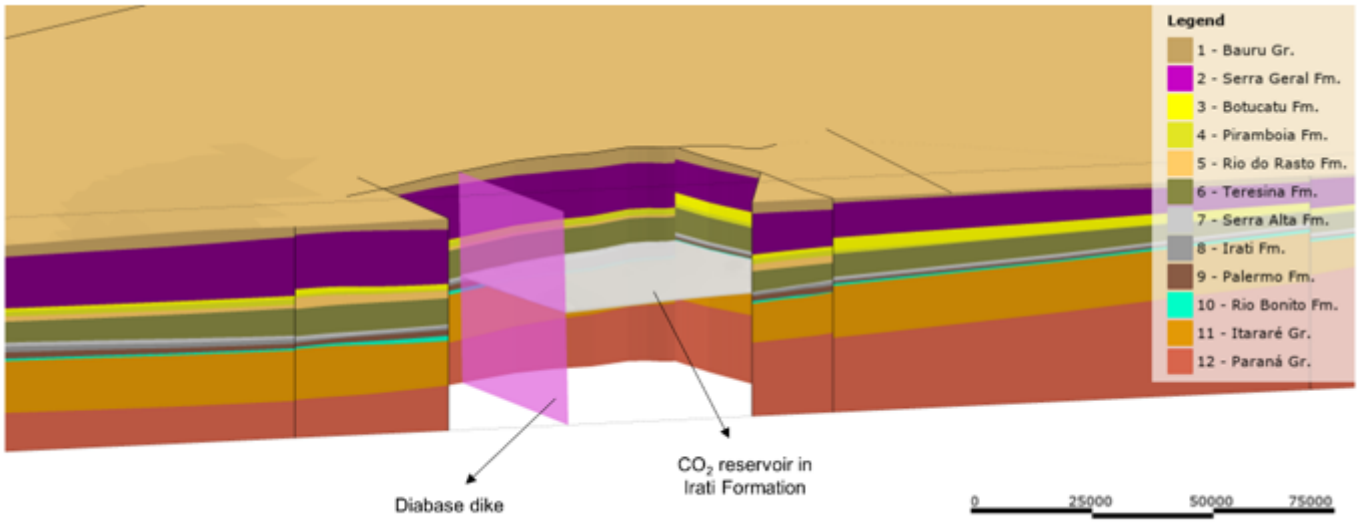

Figure 11

3D view with an E-W slice of the site location for CO2 storage used for calculation of theoretical capacity. Vertical scale = 10x.

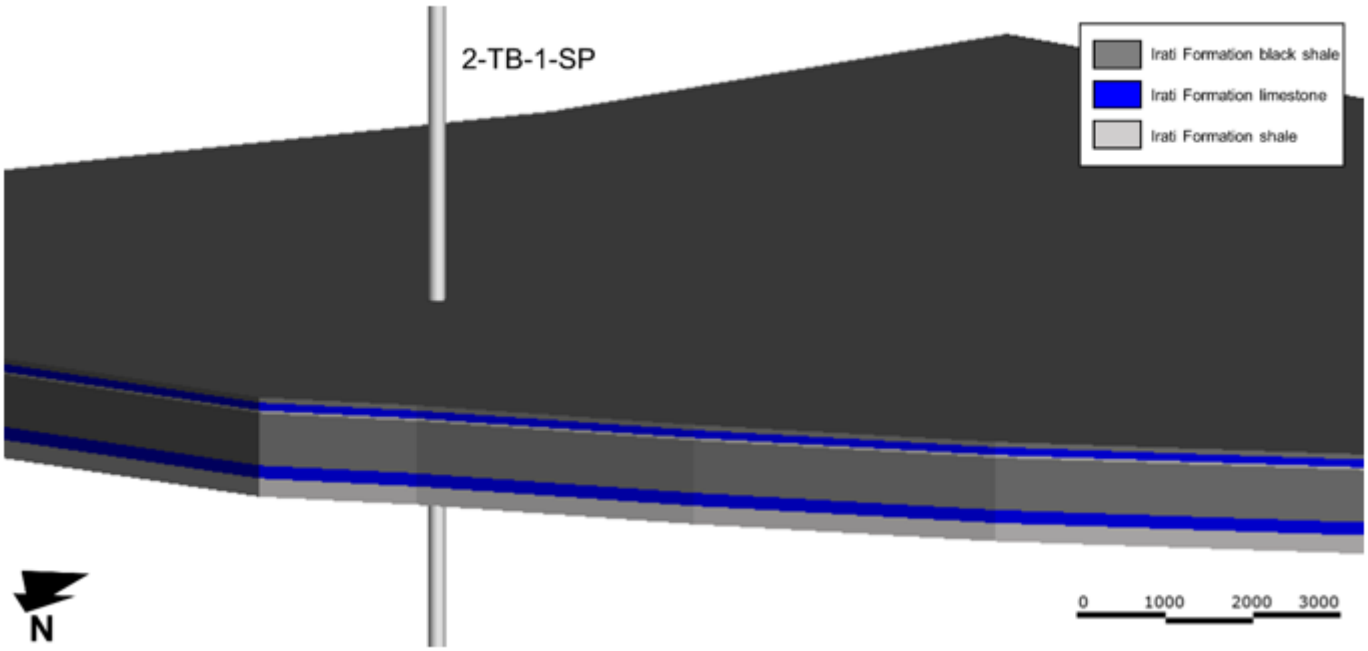

Figure 12

3D view of the local geological model of the CO2 reservoir with the 2-TB-1-SP well and geological units according to Fig. 3. Vertical scale = 30x.